

A Survey on Infrared Image & Video Sets

Kevser Irem Danaci^{1*} and Erdem Akagunduz²

^{1*}Department of Electrical Eng., Sivas University of Science And Technology, Turkey.

²The Graduate School of Informatics, Middle East Technical University, Turkey.

kiremdanaci@sivas.edu.tr; akaerdem@metu.edu.tr;

Abstract

In this survey, we compile a list of publicly available infrared image and video sets for artificial intelligence and computer vision researchers. We mainly focus on IR image and video sets, which are collected and labelled for computer vision applications such as object detection, object segmentation, classification, and motion detection. We categorise 109 publicly available or private sets according to their sensor types, image resolution, and scale. We describe each set in detail regarding their collection purpose, operation environment, optical system properties, and application area. We also cover a general overview of fundamental concepts related to IR imagery, such as IR radiation, IR detectors, IR optics and application fields. We analyse the statistical significance of the entire corpus from different perspectives. This survey will be a guideline for computer vision and artificial intelligence researchers who want to delve into working with the spectra beyond the visible domain.

Keywords: Infrared Image & Video Sets, Infrared Imagery, Survey, Deep Learning Datasets

1 Introduction

Artificial intelligence is based on data, which is the new defining element of science. In the past decade, machine learning techniques have evolved to the point where they are now capable of processing larger data sets than humans could ever imagine or possess. Particularly in the field of computer vision, large-scale data sets improve machine learning performance so dramatically that deep neural networks are able to perform as well as humans on especially high-quality images [30]. The amount of labelled visual data available for various computer vision tasks (such as image classification, segmentation, detection, tracking, etc.) has reached billions of high-quality images [125] available worldwide for use by researchers and engineers.

Visual data that is publicly accessible comes in a variety of formats. Although the available data is overwhelmingly composed of the visible band,

or in other words, “RGB” images; public access to images of other modalities, such as multi/hyperspectral, magnetic resonance (MR), computerised tomography (CT), synthetic aperture radar (SAR), to name a few, is also possible. One relatively less public imaging modality is the infrared (IR) imagery, which corresponds to images constructed with the radiation of an invisible portion of the electromagnetic spectrum, known as the infrared band.

All kinds of objects emit infrared radiation [45]. With its low radiation absorption, high contrast, and capacity for hot target detection, the IR band is popular and practical for use in civil and military applications [83]. IR imaging is used in many applications, such as object detection, object segmentation, classification, motion detection, etc. However, in contrast to visible band

imagery, IR images are difficult to access for several reasons. To begin with, the technology of most IR imaging systems is relatively expensive for use in consumer electronics. Besides, since most IR vision applications are utilised for military or medical applications, they are inaccessible due to either security reasons or intellectual property rights. As a result, the publicly available infrared image and video sets are limited compared to high-scale labelled visible band image and video sets.

The primary purpose of this article is to compile a list of publicly available infrared image and video sets for artificial intelligence and computer vision researchers. We mainly focus¹ on IR image and video sets which are collected and labelled for computer vision applications such as object detection, object segmentation, classification, and motion detection. We categorize 109 different publicly available or private sets according to their sensor types, image resolution, and scale. We describe each and every set in detail regarding their collection purpose, operation environment, optical system properties, and area of application.

The number of survey studies on IR vision algorithms and IR vision technologies is increasing [47, 48, 82, 107]. However, to the best of our knowledge, no published survey studies that review IR image or video sets exist. Our aim is to compile a collection of sets so that researchers in the fields of computer vision and deep learning can identify a visual corpus with necessary properties and compare it with other sets already available. As a result, we believe that the survey can contribute to new algorithms in deep learning and vision research using the spectra beyond the visible spectrum. By scanning public academic sources, we compile this list of image and video sets collected using IR imaging equipment. What is more, for the reader to completely evaluate the different properties of IR image and video sets, we also provide a background on the fundamentals of infrared imagery, including topics such as principles of infrared radiation, infrared sensors, infrared optics, and application fields of IR imagery.

The remainder of this paper is organised as follows: Section 2 covers a general overview of IR

radiation, IR detectors, IR optics and related applications. Section 3 starts with an analysis of the statistical significance of the entire corpora and follows by providing the compiled sets as a list with brief descriptions. Finally, Section 4 procures conclusions and sets future directions for the paper.

2 Fundamentals of Infrared Imagery

2.1 Infrared Radiation

The discovery of IR radiation dates back to an experiment by Frederick William Herschel more than 200 years ago using prisms and basic temperature sensors to measure the wavelength distribution of the stellar spectra [22]. However, its widespread use is relatively new, starting by the early 20th century with the understanding of Plank’s law and blackbody radiation, and also with the help of modern physics and quantum theory [19, 56]. Today it is almost common knowledge that according to specific known laws of physics, objects emit unique radiation in a broad region of wavelengths called the electromagnetic spectrum (ES). The IR region of this spectrum corresponds to wavelengths from the nominal red edge of the visible spectrum around 700 nanometers to 1 millimetre. IR wavelengths in this region are conventionally categorised into five spectral sub-bands. The wavelength region of $0.7\mu\text{m}$ to $1.4\mu\text{m}$ is called the near-infrared (NIR), $1.4\mu\text{m}$ to $5\mu\text{m}$: the short-wave infrared (SWIR), $3\mu\text{m}$ to $8\mu\text{m}$: the mid-wave infrared (MWIR), $8\mu\text{m}$ to $15\mu\text{m}$ the long-wave infrared (LWIR), and finally $15\mu\text{m}$ to $1000\mu\text{m}$ the far-infrared (FIR) (see Table 1).

The conventional categorization of IR sub-bands defined in Table 1 is correlated with how IR radiation is absorbed, reflected or transmitted by the atmosphere. The region of the IR spectrum, where there is relatively little absorption of terrestrial thermal radiation by atmospheric gases, is called the IR atmospheric window, which is roughly between 1 to $15\mu\text{m}$. The absorption of IR radiation depends on various atmospheric conditions such as altitude, latitude, solar Zenith angle, water vapour, etc. In Figure 1, a synthetically created spectrum of atmospheric transmission between $0.7\text{-}30\mu\text{m}$,

¹Multispectral image sets collected with satellites are left out of the scope of this survey paper. We believe that multispectral satellite imagery is a category that requires a unique focus due to differences in IR imaging in vision practices, perspective, atmospheric effects and applications.

Table 1: The IR Spectrum

Wavelength	Designation
$10^{-6}\mu\text{m}$ to $10^{-2}\mu\text{m}$	x rays
$10^{-2}\mu\text{m}$ to $0.4\mu\text{m}$	ultraviolet
$0.4\mu\text{m}$ to $0.7\mu\text{m}$	visible
$0.7\mu\text{m}$ to $1.4\mu\text{m}$	NIR
$1.4\mu\text{m}$ to $3\mu\text{m}$	SWIR
$3\mu\text{m}$ to $8\mu\text{m}$	MWIR
$8\mu\text{m}$ to $15\mu\text{m}$	LWIR
$15\mu\text{m}$ to 1mm	FIR
1mm to 1m	microwaves
1m to 10km	radiowaves

using the ATRAN module² [68] is depicted. For instance, as seen in Figure 1, atmospheric transmittance of the NIR spectrum band is relatively high, which makes this sub-band an effective spectrum for *active* (i.e. a radiation source illuminating the scene) night vision systems.

It is also seen in Figure 1 that much of the IR spectrum is not suitable for everyday applications because IR radiation is absorbed by water or carbon dioxide in the atmosphere. However, there are a number of wavelength bands with low absorption, which actually create the IR sub-bands known as the short, medium and long-wavelength IR bands, abbreviated as SWIR, MWIR and LWIR respectively.

Visible, NIR or SWIR light ($0.35\text{-}3\mu\text{m}$) corresponds to a high atmospheric transmission band and peak solar illumination. This is why most optical systems usually include detectors sensitive to these bands for the best clarity and resolution. However, without moonlight or artificial illumination, SWIR imaging systems are known to provide poor or no imagery of objects below 300K temperatures. SWIR imaging systems predominantly use reflected light. Accordingly, they are comparable to grey-scale visible images in resolution and detail.

The MWIR (also referred to as the ‘MIR’) band also provides partial regions of lossless atmospheric transmission with the added benefit of reduced ambient and background noise. This region is referred to as the “thermal infrared”. The radiation in this sub-band is emitted from the object

²ATRAN module input parameters are selected as, observatory altitude: 13800 feet (Mauna Kea (red) at an altitude of 13.8K feet and 3.4 mm water vapour), observatory latitude: 39 degrees, water vapour overburden: 0 microns, standard atmosphere with 2 Layers, Zenith angle: 45 degrees, smoothing resolution: 1000.

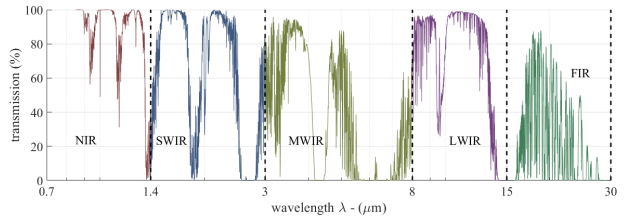


Fig. 1: Synthetic spectrum of atmospheric transmission between $0.7\text{-}30\mu\text{m}$, created with ATRAN module [68].

itself; hence passive imaging is utilised. Two principal factors determine how bright an object appears in the MWIR spectrum: the object’s temperature and its emissivity (E). Emissivity is a physical property of materials that describes how efficiently it radiates the absorbed radiation.

The LWIR band spans roughly between $8\text{-}15\mu\text{m}$, with almost no atmospheric absorption between the $9\text{-}12\mu\text{m}$ region. Because LWIR sensors can construct an image of a scene based on passive thermal emissions only and hence require no active illumination, this region is also considered as “thermal infrared”. LWIR band is better than MWIR for imaging through smoke or atmospheric particles (aerosols). Therefore, surveillance applications usually prefer LWIR technology. On the other hand, for very long-range detection (such as 10km or more), MWIR has greater atmospheric transmission than LWIR in most atmospheric conditions.

Although the FIR spectrum is defined between $0.75\mu\text{m}$ and 1mm, the atmosphere absorbs almost all IR radiation with wavelengths above $25\mu\text{m}$. Hence, atmospheric FIR spectroscopy can only be effectively utilised for wavelengths in the limited spectrum between $0.75\text{ to }25\mu\text{m}$. This region is also an atmospheric thermal band, which we can experience in the form of heat waves. For astronomical observation outside of the atmosphere, the entire FIR spectrum is utilised.

For a general overview of the subject and the fundamentals of radiometry, the reader may refer to [80].

2.2 Infrared Detectors

One of the fundamental parts of an IR electro-optical system is the detecting sensor. In order to capture the IR signature of a scene, a detector sensitive to IR radiation is needed. IR-sensitive

detectors capture the IR radiation emitted by the objects and the scene, and convert it into electrical signals. Objects that have different temperatures and emissivity, emit different levels of radiation so that the camera produces electrical signals that have different amplitudes. These electrical signals are used to produce the IR image.

Detectors are the core of an IR imaging system. Historically IR detectors can be scrutinised in three generations. The first generation consists of single-cell detectors. In order to create an image plane, the infrared beam emitted from a scene reaches a reflective surface (i.e. mirror). As the position of the mirror is deflected by two-dimensional rotary actuators, the focused infrared beam creates a two-dimensional pattern of the target image plane. In contrast, the second-generation systems comprise an array of detectors with an optical mirror system that rotates only on a single axis. Finally, the modern third-generation IR optical systems have two-dimensional array detectors, known as focal plane arrays (FPA), so that the system does not need a mirror system to scan different parts of the scene [9, 45]. Third-generation IR detectors are quite similar to modern digital photographing machines in principle.

In order to measure IR detector performance, three principle metrics are utilised: photosensitivity (or responsivity), noise-equivalent-power (NEP), and Detectivity (D^*).

Photosensitivity or responsivity is defined as the output signal per Watts of incident energy. The output may vary according to the type of detector, for example, while the output signals in photovoltaic detectors are usually photocurrent (i.e. Amperes), the output signals in photoconductor detectors are obtained as voltage. Photosensitivity is related to the magnitude of the sensor's response and is expressed as follows;

$$R = \frac{S}{PA} \quad (1)$$

where S is signal output, P is incident energy and A is the detector's active area [45, 115].

The signal-to-noise ratio (SNR) for a given input flux level is an important parameter used to determine IR image sensitivity [17]. NEP is the quantity of incident light when the SNR is 1 and expressed as follows:

Table 2: Types of Infrared Detectors

	Type	Properties
Thermal Detectors	Thermocouples, Thermopiles, Bolometers, Pneumatic cells, Pyroelectric Detectors	room temperature operation, low cost, low sensitivity, slow response.
Photon Detectors	Photoconductors, Photodiodes, Schottky Barrier Detectors, Quantum Well IR Photodetectors	low temperature operation, higher cost, higher sensitivity, fast response.

$$NEP = \frac{PA}{S/N \cdot \sqrt{\Delta}} \quad (2)$$

where N is the noise output and Δ is the noise bandwidth (and S,P and A are the same as in eq. 1).

Detectivity D^* (*normalised* detectivity) is the photosensitivity per unit active area of a detector and is expressed as follows:

$$D^* = \frac{\sqrt{A}}{NEP} \quad (3)$$

Technologically, IR detectors are classified into two main groups: thermal detectors and photon (quantum) detectors (see Table 2) [91]. Thermal detectors include thermocouples, thermopiles, pyrometers and bolometers that use infrared energy for detection. They are constructed using metal compounds or semiconductor materials and are low-cost. These detectors operate at room temperature. Their sensitivity is independent of wavelengths. Consequently, they are capable of capturing scenes in all IR sub-bands. However, they suffer from slow response times, low sensitivity, and low resolution.

In contrast to thermal detectors, photon detectors simply count photons of IR radiation. There are different technologies that operationalize these types of sensors such as photoconductors, photodiodes, Schottky Barrier Detectors, and Quantum Well detectors [91]. Compared to thermal sensors, they are more sensitive and operate faster. However, these types of detectors do not operate at room temperature but require a cooling capability. In addition, they are made from materials such as InSb, HgCdTe, and GaAs/AlGaAs whose sensitivity depends on photon absorption and, therefore are more expensive. They also have a limited IR spectrum. Photon detectors are usually utilised

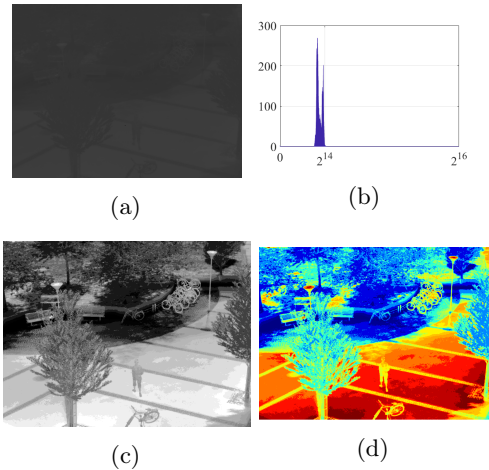


Fig. 2: (a) A 16-bit raw IR image, (b) its 16-bit raw pixel histogram (x-axis has logarithmic scale), (c) the enhanced image and (d) the false-colour image are depicted. (The picture is taken from The LTIR Dataset [12])

when a high-sensitivity response is required at a specific wavelength.

Comparative studies on thermal and photon detectors show that both sensor types have their pros and cons [50, 91, 115]. Photon detectors are favoured at specific wavelengths and lower operating temperatures, whereas thermal detectors are favoured at a very long spectral range [90]. Photon detectors are fundamentally limited by generation-recombination noise arising from photon exchange with a radiating background. Thermal detectors are fundamentally limited by temperature fluctuation noise arising from radiant power exchange with a radiating background [61].

2.2.1 IR Detector Raw Output

The raw pixel output of an IR detector is the irradiance (i.e. the flux of infrared energy per unit area) transformed into quantised n -bit values. These values are within the limits of the so-called “dynamic range”, which is the difference between the largest and smallest signal value the detector can record or reproduce. Hence, the raw pixel values are usually not uniformly distributed within the dynamic range. In practice, a raw IR detector output is usually confined to a very limited range. In Figure 2, a 16bit IR detector raw output (taken from [12]),

its 16-bit raw pixel histogram and the enhanced image are depicted.

IR electro-optical systems that provide a visual output for human users, enhance the raw detector output using contrast-enhancing histogram shaping methods [101]. These types of systems usually provide 8-bit contrast-enhanced images as output. The aim of such a process is to increase the contrast of the raw IR image for the human observer. As seen in Figure 2a, the raw image is barely visible to the human eye. Due to the irreversibility of most image enhancement algorithms, the bit range decreases with the price of sacrificing information. This enhancement is usually a default process for visible band cameras. On the other hand, systems that provide intelligent IR image processing algorithms, such as tracking, detection, recognition, etc., utilize the raw output of pixels; since the raw output is representative of the actual irradiance values collected from the scene and has a higher dynamic bit range. The raw output of the electro-optical system usually has the same bit-depth as the IR detector, such as 11-bits or 14-bits. In the following section, when analyzing the various image and video sets, information regarding the raw or enhanced nature of pixel values for a given set is specifically indicated.

Some thermal cameras utilize false colours for their 8-bit contrast-enhanced output. This is usually done for temperature mapping for cameras that are used for temperature measurement. In Figure 2d, an example of a false-colour contrast-enhanced infrared image is depicted.

2.3 Infrared Optics

IR imaging technology was founded in the late 1920s with the understanding of photon emission, and improvements continue even today [19]. IR imaging is based on a fundamental concept in geometrical optics called the ray model. A ray model ignores the diffraction and assumes that light travels in straight lines from a source point. Each location in the scene can be assumed as a source point, and the source points emit different levels of radiation that create the IR scene.[17].

In geometrical optics an image is constructed via an optical material, by focusing the rays collected from the scene onto an image plane. Hence, the optical material used in an infrared system needs to be transparent (i.e. with transmittance

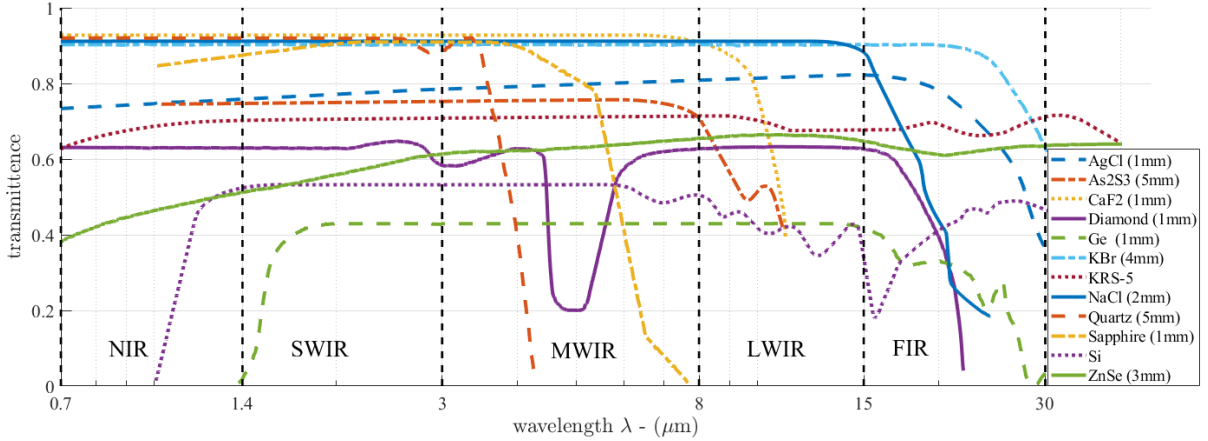


Fig. 3: Transmittance of different materials in IR sub-bands.

closer to 1.0) at the wavelength the detector is sensitive to. The percentage of incident light that passes through a material for a given wavelength of radiation is defined as electromagnetic transmission, also known as transmittance.

When choosing the correct optical material for an IR imaging system, there are three main points to consider. The first is the thermal properties of the material. Optical materials are typically placed in environments with varying temperatures, and as a result, they can generate a significant amount of heat. To ensure that the user receives the desired performance, the coefficient of thermal expansion (CTE) of the material should be evaluated. Secondly, as mentioned above, sufficient transmittance of the material for the given wavelength is a must. In Figure 3, the transmittance of different materials in IR sub-bands is depicted. For example, if the system is intended to operate in the LWIR band, germanium (Ge) optics with a thickness of 1mm are preferable to sapphire optics with the same thickness.

Another factor in choosing a suitable optical material is the refractive index, which is the measure of how fast radiation travels through a material. IR refractive index varies among materials, allowing more flexibility in system design. As a solution, anti-reflection coatings are applied to materials used for IR optics, which also limits them to a desired band within the IR spectrum.

For more information on the subject, the reader may refer to [27].

2.4 IR Electro-Optical System Properties

There are some important parameters used in selecting appropriate equipment and characterising the performance of IR systems. The parameters that measure the performance of an IR electro-optical system depend on its ability to detect IR radiation and resolve the temperature differences in the scene. The contrast in an IR image occurs due to variations in temperature and emissivity. The parameters that may affect the performance of an IR electro-optical system, in general, include spectral range, normalised detectivity, temperature range, absolute accuracy, repeatability, frame rate, spatial resolution and thermal sensitivity [113]. Below these parameters are briefly explained:

- *Spectral range*: refers to the wavelength range in which the IR system will operate.
- *Normalised detectivity* (D^*): as defined in eq. (3), is one of the widely used parameters to compare the performance of IR detectors.
- *Temperature range*: or the *operating temperature*, is the minimum and maximum temperatures that can be measured by the IR electro-optical system. It has a unit of K, $^{\circ}\text{C}$, or $^{\circ}\text{F}$.
- *Absolute Accuracy*: is a measure of how accurately the system detects the actual temperature and is denoted by temperature units. Related to this measure, *Repeatability* is defined as the consistency of the system accuracy.

Table 3: A selection of commercial NIR electro-optical systems and their properties.

Cameras → Parameters ↓	FLIR A35	FLIR T560	FLIR A655SC	FLIR T1010	FLIR A65	FLIR E8-XT
<i>Spectral Range</i>	7.5–13 μm	7.5–14 μm	7.5–14 μm	7.5–14 μm	7.5–13 μm	7.5–13 μm
<i>Detector Type</i>	Uncooled VOx μ -bol.	Uncooled μ -bol.	Uncooled μ -bol.	Uncooled μ -bol.	Uncooled VOx μ -bol.	Uncooled μ -bol.
<i>Field of View (lens size if available)</i>	63°x50°(7.5mm) 48°x39°(9mm) 24°x19.2°(19mm) 13°x10.8°(35mm) 7.6°x6.08°(60mm)	14°x10°	15°x11°	12°x9°	90°x69°(7.5mm) 45°x37°(13mm) 25°x20°(25mm) 12.4°x9.92°(50mm) 6.2°x4.96°(100mm)	45°x34°
<i>Thermal Sensitivity (NETD)</i>	<0.05°C @ 30°C / 50 mK	<50 mK @ 30°C	<30 mK	<25 mK @ 30°C	< 50 mK @ 30°C	<0.05°C /<50 mK
<i>Object Temperature Range</i>	-25↔135°C -40↔550°C	-20↔120°C 0↔650°C 300↔1500°C	-40↔150°C 100↔650°C	-40↔650°C	-25↔135°C -40↔550°C	-20↔550°C (-4↔1022°F)
<i>Measurement Accuracy</i>	± 5°C (± 9°F) or 5 % of reading	±2°C or ±2% of reading	±2°C or ±2 % of reading	± 2 °C or ± 2% of reading	± 5°C (± 9°F) or 5 % of reading	±2°C (±3.6°F) or ±2% of reading
<i>Operating Temperature Range</i>	-15↔60°C	-40↔75°C	-15↔50°C	-15↔50°C	-15↔60°C	-15↔50°C

- *Frame rate*: is the number of frames displayed per second. For monitoring moving objects, higher frame rate cameras are mostly preferred [9]. It has a unit of Hz.
- *Spatial resolution*: also referred to as the “instantaneous field-of-view” (IFOV), is the imaging system’s ability to differentiate the details of objects within a single pixel-sized FOV. It is a measure of solid angle, hence represented by steradians. As spatial resolution increases, so does the image quality [9].
- *Thermal sensitivity*: is the smallest temperature change detected by the IR imaging system. There are three most common parameters used as a measure of thermal sensitivity, namely “Noise Equivalent Temperature Difference” (NETD), “Minimum Resolvable Temperature Difference” (MRDT) and “Minimum Detectable Temperature Difference” (MDTD) [113]. It has a unit of temperature (i.e. K, C°, or F°).

In order to choose the right camera for the right application, all of the aforementioned parameters should be taken into account. There are numerous commercial IR electro-optical systems available in the market. In Table 3, we provide a selection of six different near-infrared electro-optical systems, with their comparative parameters, so as to give the reader a sense of the systems engineering perspective of IR electro-optical system selection.

2.5 Applications of IR Electro-Optical Systems

The development in IR sensing technologies has resulted in countless applications, which we divided into four major categories: military & surveillance, industrial, medical, and scientific. Each category title is briefly explained below. The IR image and video sets provided in the next section are categorised according to these application titles.

- *Military & Surveillance Applications*: The military and surveillance field, which also encapsulates law enforcement and rescue applications, cover a wide variety of applications utilised in all IR sub-bands. Warfare applications include target tracking/detection/acquisition in various platforms such as missile seeker heads, forward-looking infrared (FLIR) systems, infrared search and track (IRST) systems, and directional countermeasure (DIRCM) systems. Regarding law enforcement and rescue applications, night vision systems, reconnaissance and surveillance, fire fighting and rescue in smoke, identification of earthquake victims’ locations, forest fire detection, and radiation thermometer are prime examples.
- *Industrial Applications*: Industrial applications of IR imaging systems include the utilization of IR sensing technology in various industrial

fields, such as infrared heating in process control, nondestructive inspection of thermal insulators, hidden piping location detection, diseased tree and crop detection, hot spot detection, brake lining, industrial temperature measurement, clear-air turbulence detection, pipeline leak and petrol spill detection, just to name a few.

- *Medical Applications*: In medicine, IR technology is fundamentally used for diagnosis, such as early cancer detection, determining the optimum site for amputation, determining the location of the placenta, detecting strokes and vein blockages before they occur, monitoring wound healing, and detecting infection. Due to its non-invasive nature, IR technology in medicine provides information about conditions that are directly or indirectly related to the focused region of the body (such as hands [102]), as well as facilitating the assessment of treatment.
- *Scientific Applications*: In nearly every scientific field, from remote sensing and meteorology to material science and microbiology, from engineering to biology, IR imaging technologies are used. In this paper, when categorizing a set as "scientific", we took into account its use outside of the other categorised sectors, namely military, surveillance, industrial, and medical. An image or video set, for example, is classified as both Military & Surveillance and Scientific if it has the capacity to support both types of applications.

3 IR Image & Video Sets

The paper analyses 109 IR image and/or video sets and provides a list of the sets in Table 4. A total of 77 are public, in other words, they offer public download links, while 3 are private and require payment. The remaining 29 sets can be downloaded for free but require manual registration by contacting the institution that owns them. The entire corpus of sets includes nearly 20 million still images and video frames. In the following, we provide the statistical details of the compiled list of IR image and video sets in terms of application fields, included object categories, resolution, annotation, and pre-processing, before presenting the list with brief descriptions.

Table 4 provides a sample image and a brief description for every set. There are also separate columns for technical details, such as types of

annotated classes, number of total frames, image resolutions, sensor types, image bit depths, and application fields. The description section additionally specifies whether the collection is accessible to everyone (pub), accessible to paid users only (pri), or needs registration (rr). For more details, we suggest that the reader consult the References section for an online link to the image set.

3.1 Application Fields

As mentioned in the previous section, application fields for IR image and video sets are scrutinised in 4 main titles: Military & Surveillance (Mil. & Sur.), Industrial, Medical and Scientific. As seen in Figure 4a, Military & Surveillance comprises 65.2% of the total volume of images and video frames, clearly demonstrating the importance of IR imaging in this industry. Sets collected for scientific applications cover 25.9% of the corpus, while medical applications cover 8.6%, most likely due to the legal challenges involved in collecting or publishing health informatics data. Industrial applications account for a marginal share, which is probably due to the fact that they do not publish their data in public domain. In Table 4, the application fields for every individual set are indicated in the right-most column (titled "App.").

3.2 Resolution and Sensor

IR image and video sets listed in this survey range from *lower*-definition (LD--), which corresponds to resolutions lower than LD, to *ultra-higher*-definition (HD++), which corresponds to resolutions higher than UHD. Depending on the application, the resolution plays a significant role. Most surveillance systems require HD or better resolutions for accuracy. On the other hand, LD and standard definition (SD) systems are ideal when the computational capabilities of the system are limited. Figure 4b shows that despite three-quarters of the corpora being SD++ or worse, the rest are almost UHD or better. It is important to note that sets with UHD or better resolutions are recent sets showing a clear future trend. In Table 4, the actual resolutions for every individual set are indicated in column four (titled "res").

In addition, the optical equipment used to collect each set is provided in column five (titled "Sensor"). When compared to RGB cameras, IR optical systems are capable of different kinds of

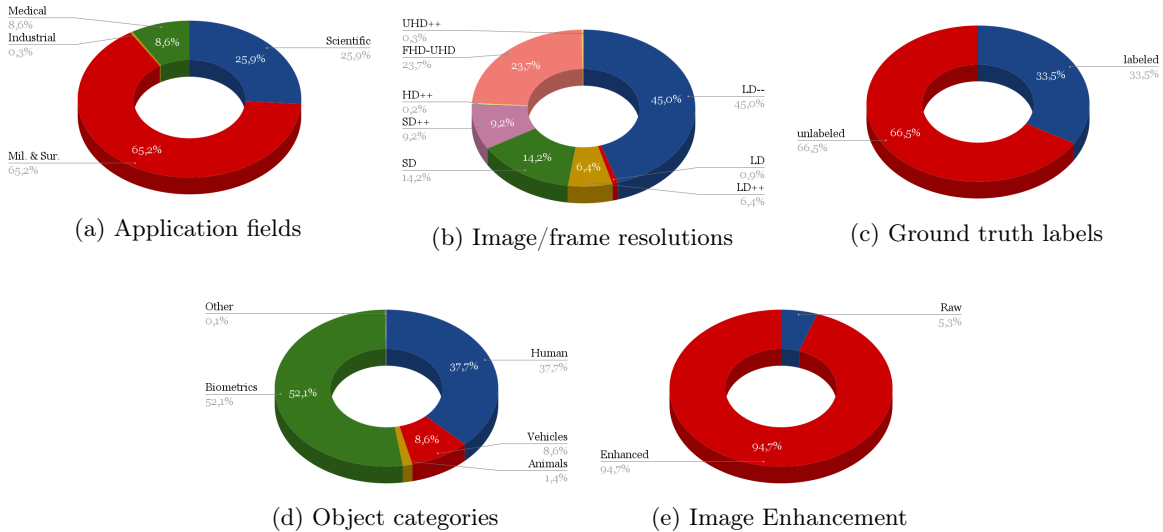


Fig. 4: Distributions of various attributes (application field, resolution, ground truth labelling, object category and image enhancement) in the entire collected image/frame corpus are depicted in pie charts.

calibration, and they are capable of producing characteristic output that may not be replicated with similar equipment. The reason for this is that today’s RGB cameras usually use the same pre-processing and aim at producing almost the same output, whereas, with IR vision, it becomes important to know the parameters of the equipment in order to recreate similar scenes or images. Therefore, in Table 4 column titled “*Sensor*”, we provide details regarding the collection equipment for the sets, which openly specify these details.

3.3 Annotations and Object Categories

Many computer vision applications annotate data with labels for certain purposes, such as detection, tracking, and recognition. Data annotation/labelling is an expensive effort, which provides means for supervised learning, and hence deep learning if the annotated data are sufficiently large in scale. Similarly, some of the IR sets listed in this survey are annotated with various labels. As shown in Figure 4c, about 33.5% of the entire corpus is annotated. For some sets, these annotations are black-box locations for objects, whereas for others they are global labels for entire images. A majority of the corpora are not labelled, but we believe that most annotations may not be shared publicly due

to their commercial implications. Once again, it is important to note that sets with labels are recent sets showing another future trend.

In Table 4, (in column three, titled “*Classes*”), categories for any existing annotation of a given set are provided. The entire collection of sets includes a wide range of object annotation categories. The objects are categorised under seven titles in Figure 4d, namely biometrics, environments, humans, vehicles, animals, unknown and uncategorised. Biometrics annotations include IR images of faces, irises, ears and/or fingerprints, and cover the majority of the annotations with a 52.1% share. Human annotations, including pedestrians, runners, sportsmen, etc cover 37.7% of these annotations. Vehicles of different sorts such as cars, bicycles, motorcycles, aircraft, boats, etc, are also included and cover 8.6% of label annotations. There are a small number of animal class annotations that take 1.4%. There is also a marginal share of annotations that are related to environmental objects, including terrain, roads, clouds, or various objects like food, or uncategorised application-specific labels.

3.4 Image Enhancement

As mentioned previously in Section 2.2.1, IR electro-optical systems that provide a visual output

for human users, usually enhance the raw detector output using contrast-enhancing histogram shaping methods. However, IR image processing systems that utilize algorithms such as tracking, detection, recognition, etc., utilize the raw output of pixels, which usually has the same bit-depth of the IR detector. The histogram-enhanced image is, in most cases, the only accessible output of an IR optical system. For such systems, the details of the enhancement algorithms are rarely provided to the user. Most systems apply different algorithms that suit their design requirements such as level of contrast, and real-time operation, just to name a few. As seen in Figure 4e, only a minority of 5.3% of the entire corpora of collected frames are raw detector outputs. The “bit” column in Table 4 gives information about the bit depth of an image/frame for a given set. The number (8, 11, 16, etc.) corresponds to image bit-depth. For some sets, the bit depth is indicated by “8*” showing that the images/frames are of 24bit RGB (i.e 8bit per channel) format. The abbreviation “HE” is to indicate the existence of any histogram enhancement process, whereas “RAW” suggests the accessibility of the raw detector output. The type of enhancement technique is not indicated in the table, because this information is not available for most of the collection equipment.

4 Conclusions and Future Directions

In this survey, we compile a list of publicly available IR image and video sets for artificial intelligence and computer vision researchers. We mainly focus on IR image and video sets, which are collected and labelled for computer vision applications such as object detection, object segmentation, classification, and motion detection. We categorize 109 publicly available or private sets according to their sensor types, image resolution, and scale. The list includes brief descriptions for each set. The statistical details of the entire corpus of IR image & video sets are provided in terms of applications fields, including object categories, resolution, annotations, sensor types and preprocessing details.

We believe that this survey, with solid introductory references to the fundamentals of IR imagery,

will be a guideline for computer vision and artificial intelligence researchers who want to delve into working with the spectra beyond the visible domain. Today, consumer electronics are integrating IR cameras with smartphones, making IR imaging a reality within the consumer market. Within a short time, the IR domain will host a large number of pre-trained deep learning models. Therefore, this collection can be used to research deep learning models for vision problems like IR domain adaptation, multi-modal vision, and fusion in the future. Such an approach may result in IR subband-specific deep feature extractors, which can be used for a variety of vision tasks. These models would need very large-scale sets. A crucial practice in the future would be the ongoing updating of this survey, especially in light of the possibility that annotated IR sets may soon be made available in vast quantities.

Declarations

The authors have no conflicts of interest to declare that are relevant to the content of this article.

Data Availability Statement

The dataset generated during the current study is available from the corresponding author upon reasonable request.

References

- [1] (2018) Multi-modal dataset for hand gesture recognition. Available at <https://www.kaggle.com/gti-upm/multimodhandgestrec>
- [2] (2020) Thermal images - diseased and healthy leaves - paddy. Available at <https://www.kaggle.com/sujaradha/thermal-images-diseased-healthy-leaves-paddy?select=thermal+images+UL>
- [3] Akula A, Khanna N, Ghosh R, et al (2014) Adaptive contour-based statistical background subtraction method for moving target detection in infrared video sequences. *Infrared Physics and Technology* 63:103–109. Available at <http://vcipl-okstate.org/pbvs/bench/>

Table 4: From left to right, the columns depict the name and the reference, a sample image, the included object classes (if any), total number of frames, pixel resolution of images, the optical system (if specified), pixel bit depth (and if any histogram equalization - HE applied), a brief description and the application fields of the given dataset, respectively.

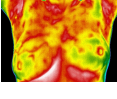
Name	Sample	Classes	# fr.	res.	Sensor	bit	Description	App.
AAIart Data [124]		pedestrian, vehicle	771	640x513	Catherine MP LWIR	8 HE	(pub) The dataset includes thermal infrared video sequences comprising of pedestrians and various types of vehicles for an infrared surveillance system that can be widely applied in military applications.	Mil. & Sur.
AAU RainSnow [10]		vehicle	4.5K	640x480	not specified	8* HE	(pub) The image set includes traffic surveillance images (RGB+thermal) and 22 video pairs in rainfall and snowfall from seven different traffic intersections at the Danish cities of Aalborg and Viborg. The purpose of the dataset is detection and classification under challenging weather conditions. The dataset includes pixel-level annotations of 2,200 frames, containing 13,297 objects.	Mil. & Sur.
AAU-PD-T [49]		pedestrian	3K	384x288 640x480	Axis Q1921 Axis 1922	8* HE	(pub) The image set contains approximately 3k thermal pedestrian images with a total of 5590 person annotations. Training data is divided into 9 categories, such as good weather, far viewpoint, occlusions, snow, wind, just to name a few.	Mil. & Sur.
All-Ther [8]		vehicle, pedestrian	20K	640x512 1280x1024	not specified	8* HE	(pub) The thermal dataset contains vehicle and pedestrian infrared images in traffic and parking land scenarios. The set provides bounding box annotations.	Mil. & Sur.
ASL-TIR [84]		human, cat, horse	4381	324x256	FLIR Tau 320	8/16 HE/RAW	(pub) ASL thermal IR dataset includes 8 sequences of thermal images of humans, cats and horses, with annotations. The images are captured at indoor and outdoor environments.	Mil. & Sur.
Baracca [92]		person	9600	160x120 640x480	Pico Zense DCAM710 PureThermal 2	8 HE	(rr) The dataset presents depth, thermal and RGB images for anthropometric measurements such as height, shoulder width, and forearm with annotations.	Scientific
BCT [39]		breast	60	640x480	Infrac R500	8 HE	(pub) The dataset contains thermal breast images of 60 patients for breast cancer detection.	Medical
BERTIN [26]		vehicle, pedestrian	more than 10K	320x240	FLIR A20M	16 RAW	(rr) The dataset includes both visible and thermal images of pedestrians and vehicles, captured with a static and a moving camera. Contains training, validation and test sets with their ground truths.	Mil. & Sur.
Bird [5]		bird	302	416x416	not specified	8* HE	(pub) The dataset presents thermal images that include flying birds with annotations.	Scientific

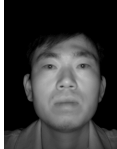
Table 4		continued...							
BIRDSAI [116]		human, animal	160K	640x480	FLIR Vue Pro 640 Tamarisk 640	8 HE	(<i>pub</i>) The dataset consists of two parts: real and synthetically-created, with annotations. The real data includes 48 thermal infrared videos sequences of humans and animals, captured with a thermal camera mounted on a UVA, that flies over African landscapes. The synthetic data, generated with MS Air-Sim simulation platform, include 124 thermal infrared video sequences.	Scientific	
BU-TIV [119]		motorcycle, runner, car, bicycle, pedestrian	35K 2999 6000 1275 1282	up to 1024x1024	FLIR SC8000	16 RAW	(pub) The dataset contains various tasks, such as single object detection, multi-object detection, motion detection, counting, that describes real world scenarios such as a marathon runner, people walking down a hall, etc., with ground truth data. In addition, the set includes images of bats for tracking and counting purposes.	Mil. & Sur.	
		bat	19K					Scientific	
CAMEL [38]		biker, vehi- cle, pedes- trian	44.5k	336x256	FLIR Vue Pro	8* HE	(pub) The dataset contains 26 video sequences, captured in an urban environment, in the visible and thermal infrared domains, with their annotations.	Mil. & Sur.	
Carl Database [33]		face	7380	640x480	TESTO 880-3	8* HE	(rr) Contains visible and thermal images of human faces, with a constant 135 cm distance from the sensor, in front of a matt black background.	Mil. & Sur.	
CATS [117]		vehicles, pedes- trians, other	1520	640x480	Xenics Gobi 640 GigEs	16 RAW	(pub) The dataset contains stereo thermal, stereo colour, and cross-modality images of pedestrians, vehicles, and some other objects in different weather conditions.	Mil. & Sur.	
CBSR NIR [64]		face	4K	480x640	not specified	8 HE	(pub) The dataset contains NIR images from 197 people, collected for face detection, eye detection and face recognition tasks.	Mil. & Sur.	
CDW 2014 [116]		pedestrian	21K	320x240 → 720x576	not specified	8* HE	(pub) The 2014 CDnet dataset, which is extended version of CDnet 2012 dataset, contains 11 video categories, one of which is the Thermal category, that contains 5 video sequences (3 outdoor + 2 indoor) shot by a far infrared camera annotated with pedestrian bounding boxes.	Mil. & Sur.	
Cheetah [89]		cheetah	129	416x416	Seek Compact XR	8 HE	(pub) This dataset is a collection of thermal infrared images and video frames of cheetahs.	Mil. & Sur.	

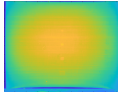
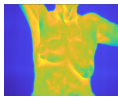
Table 4	continued...								
Comp-Mat [31]		composite materials	2000	512X512	FLIR X6900	8 HE	(pub) The dataset consists of 12 image sequences collected for locating laminar defective regions from composite materials. The IR camera records the thermal evolution of both sides of the sample for a few seconds for 3 stages, before a heat pulse, during the heat pulse and after the heat pulse.	Industrial	
CSIR CSIO [3]		vehicle, human, dog, bird	3650	640x480	Uncool. μ -bol	8* HE	(pub) A moving object detection dataset which has 18 sequences of moving targets, four, three and two-wheelers, pedestrians and some animals. Thermal infrared videos were captured at the coastal area of the Bay of Bengal in Southern India with a sampling rate of 10hz.	Mil. & Sur.	
CVC-09 [100]		pedestrian	10K	640x480	not specified	8 HE	(pub) FIR Sequence Pedestrian Dataset include two sequences, day and night, captured at urban areas. Each sequence has about five thousand frames, divided into distinct train and test sets.	Mil. & Sur.	
CVC-14 [42]		pedestrian	8400	471x640	not specified	8 HE	(pub) Visible-FIR Day-Night Pedestrian Sequence dataset includes two sequences of 3695 day images and 3390 night images, with pedestrians annotated, again divided into distinct train and test sets.	Mil. & Sur.	
DDPM [103]		face	8M	80x60 1920x1080	DMK 33UX290 FLIR C2	8 HE	(rr) The dataset includes RGB and IR face videos of 13 hours of recordings of 70 subjects, for an interview scenario, in which the interviewee attempts to deceive the interviewer on selected responses. Besides the RGB and IR videos, the set includes various biometric sensor records.	Mil. & Sur.	
DIAST [6]		ear	2200	125x125	FLIR E60	8 HE	(pub) The DIAST dataset contains visible and thermal ear images taken from a side face profile, from 55 subjects, collected for the task of ear recognition.	Mil. & Sur.	
Dim Small Air. [51]		aircraft	16K	256x256	not specified	8* HE	(pub) The dataset includes 22 sequences with sky and open-field backgrounds for infrared aircraft detection and recognition tasks.	Mil. & Sur.	
DMR-IR [114]		breast	1522	640x480	FLIR SC-620	8 HE	(pub) The dataset consists of thermal breast images to be used for breast cancer diagnosis.	Medical	
Dogs [76]		pedestrian, dog	203	416x416	Seek Compact XR	8 HE	(pub) The dataset includes thermal infrared person and dog images captured in outdoor environments.	Mil. & Sur.	
Drones [58]		drone	150	416x416 640x480	not specified	8* HE	(pub) The dataset contains thermal images for detecting UAVs. It provides ground truth bounding boxes for drones.	Mil. & Sur.	

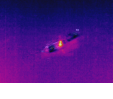
Table 4		continued...						
EADS [26]		plane, vehicle	not specified	not specified	not specified	8 HE	(<i>rr</i>) The dataset contains aerial images of vehicles, planes etc, for object detection tasks. Training and validation sets are provided with ground truths.	Mil. & Sur.
ESPOL FIR [87]		person, vehicle, objects	101	640x512	FLIR TAU 2	8 HE	(<i>pub</i>) The dataset contains infrared images taken in outdoor and indoor environments during the day. The dataset is primarily intended for super-resolution problems in the IR domain.	Mil. & Sur.
Focus-Obj [32]		circuits, heater, face, hand, etc.	960	160x120	TESTO 880-3	8 HE	(<i>rr</i>) The database consists of several image sets. In each set, the camera acquires one image of the scene at 96 different lens positions.	Industrial
FREE FLIR [34]		vehicle bicycle dog pedestrian	14K images 10k short videos	up to 1280x1024	IR Tau2 FLIR BlackFly	8/14 HE/RAW	(<i>rr</i>) The dataset contains 8 bit RGB and 8/14 bit thermal images images, with annotations. The images are captured on streets and highways of Santa Barbara, CA area, in different weather conditions, during day and night.	Mil. & Sur. Industrial
FV-USM [72]		Finger Vein	5904	640x480	not specified	8* HE	(<i>rr</i>) The dataset contains infrared finger images of 83 male and 40 female volunteers for finger vein recognition tasks.	Mil. & Sur.
HGRD [69]		hand	20K	640x240	not specified	8 HE	(<i>pub</i>) The Hand Gesture Recognition Dataset (HGRD) includes NIR images of 10 different gestures, performed by 10 different subjects (5 men and 5 women). It has 200 frames for each subject and each hand gesture.	Industrial
HS-NIR [44]		coffee bean, sugar, floor, salt	480	192x256	AHS- U20MIR	8 HE	(<i>pub</i>) The dataset provides a total of 480 images of 5 objects. For each object, there are 96 different NIR hyperspectral images.	Industrial
IIT Delhi [62]		face	612	768x576	not specified	8 HE	(<i>rr</i>) The database contains face images, captured at IIT Delhi campus with a webcam, shot with NIR-only illumination.	Mil. & Sur.
Illegal Fishers [4]		fishing gear, ship	84	640x480 4056x3040	not specified	8* HE	(<i>pub</i>) The dataset has raw thermal, visible, and night vision images captured by a drone with a thermal camera to detect the illegal fishing in Kuwaiti Bay.	Mil. & Sur.
Indoor-Outdoor IR [73]		person, vehicle, objects	400	384x288	Thermoteknix Miricle 110KS	8* HE	(<i>pub</i>) The dataset presents indoor and outdoor IR-visible image pairs. The authors captured the images to compare the statistics of the visible and infrared images.	Mil. & Sur.

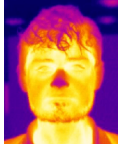
Table 4		continued...							
InfAR [36]		person	3.6M (600 vid.)	293×256	GUIDIR IR300	8* HE	(<i>pub</i>) The first publicly available dataset for infrared action recognition contains video action classes such as walking, hopping, fighting, etc. There are 12 human action classes, each with 50 videos.	Mil. & Sur. Scientific	
IPATCH [81]		boat	not specified	640×480 640×512	FLIR SC655 FLIR A65	not specified	(<i>pri</i>) The IPATCH dataset contains 14 thermal videos from the coast of Brest, France, for object detection and tracking, event detection, and threat recognition tasks of maritime piracy. There are selected sequences of abnormal events, such as boat speeding up, boat loitering, boat moving around vessel, etc.	Mil. & Sur.	
IRIS [57]		face	4228	320×240	Raytheon Palm IR Pro	8* HE	(<i>pub</i>) The dataset consists of thermal and visible face images with various expressions, poses and illumination conditions.	Mil. & Sur.	
IRShips [118]		ship	972K	1024×512	N/A	8 HE	(<i>pub</i>) This dataset contains synthetically generated IR images of 10 different ships.	Mil. & Sur.	
JPL [53]		sand, soil, rocks, bedrock, rocky terrain, etc.	1300	800×600	FLIR AX65	8 HE	(<i>pub</i>) The dataset comprises IR and RGB images, in 2 parts: 1) the Semantic Dataset for Terrain Types and 2) the Virtual Sensor Dataset for deriving RGB-to-IR mapping models. Semantic Dataset includes manually annotated 7 categories: unlabeled, sand, soil, rocks, bedrock, rocky terrain, and ballast.	Scientific	
KAIST [52]		pedestrian	95K	320×256	FLIR A35	8 HE	(<i>pub</i>) The dataset contains multispectral images of vehicles captured in day and night traffic with annotations.	Mil. & Sur.	
Kayak Image Fusion [108]		kayak	2541	up to 752×582	Raytheon Rad. HS, AEG AIM 256 PLW, Philips LTC500	8-8* HE	(<i>pub</i>) This dataset includes sequences with several kayaks in a maritime environment. The images are captured in MWIR, LWIR and visible domains.	Mil. & Sur.	
L-CAS FACE [25]		face	3000	382×288	Optris PL-450	8 HE	(<i>rr</i>) The dataset comprises of thermal images of moving faces, captured with a sensor that is mounted on the top of a robot to measure respiration and heart-beat rate for physiological monitoring. The dataset provides ground truth for respiration and heartbeat.	Mil. & Sur.	
L-CAS ReID [24]		person	36K	382×288	Optris PL-450	8 HE	(<i>rr</i>) The dataset includes RGB, depth, and thermal images of people for re-identification tasks. The set is collected via a thermal camera on a robot.	Mil. & Sur.	
Leaves [2]		leaf	636	320×240	FLIR E8	8 HE	(<i>pub</i>) The dataset, composed of thermal leaf images, is categorised into 6 categories: bacteria leaf blight, blast, leaf spot, leaf folder, hispa, healthy leaves.	Industrial	

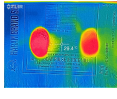
Table 4		continued...							
LLVIP [54]		person, vehicle	31K	1920×1080 1280×720	Hikvision DS-2TD8166 75C2F/V2	8 HE 16 RAW	(<i>rr</i>) Contains infrared and visible images of pedestrians in low-light conditions. The images contain vehicles, but pedestrians are only labelled. Raw data can also be obtained.	Mil. & Sur.	
LR-MR-HR FIR [88]		person, animal, vehicle, objects	3063	up to 640×512	Axis Domo P1290 Axis Q2901-E FC-6320 FLIR	8 HE	(<i>pub</i>) The dataset contains thermal images at different resolutions for image super-resolution tasks. Various levels of resolution are available: low, medium and high resolution, which correspond to 160×120, 320×240, and 640×512 pixels, respectively. There are 1021 images per resolution.	Mil. & Sur.	
LSI [77]		pedestrian	20K	32×64 164×128	Indigo Omega	14 RAW	(<i>pub</i>) The set consists of FIR pedestrian images in an outdoor urban environment, divided into train and test sets, with manually annotated bounding boxes.	Mil. & Sur.	
LSOTB TTR [67]		person, animal, vehicle, aircraft, boat	600K	not specified	not specified	8 HE	(<i>pub</i>) Contains various object classes with 730K bounding box annotations, shot in various environments, including urban areas, forests, the sea, etc.	Mil. & Sur.	
LTIR [12]		rhino, human, horse, car, quadcopter, dog	11K	up to 1920×480	FLIR A35 FLIR Tau320 FLIR A655SC	8/16 HE/RAW	(<i>pub</i>) The dataset includes 20 thermal IR sequences of different objects, captured at indoor and outdoor environments, with annotations.	Mil. & Sur.	
Mango [74]		mango	309	640×480	FLIR One	8* HE	(<i>pub</i>) The dataset consists of thermal mango images for object counting and colour feature extraction tasks.	Industrial	
MBD [95]		fingerprint, finger-vein, face, iris	72	up to 640×480	not specified	8/8*/32 HE	(<i>pub</i>) The set includes 45 thermal fingerprints, 9 thermal finger veins, 9 thermal iris, and 9 thermal face images.	Mil. & Sur.	
MBDA [26]		plane, helicopter, vehicle, tower	>15K	320×240 256×256	N/A	14/16 RAW	(<i>rr</i>) The dataset contains computer-generated aircraft and vehicle images. Train and validation sets are provided with ground truths.	Mil. & Sur.	
METU [122]		various objects	24	640×480	Kinect	8 HE	(<i>pub</i>) METU Kinect dataset consists of IR and visible image pairs of various objects.	Scientific	
MIntPAIN [46]		person, face	2M (9366 vid.)	640×480	Axis Q 1922	8 HE	(<i>rr</i>) The MIntPAIN is an RGB, Depth and Thermal (RGBDT) image set, which contains RGBDT videos of 20 subjects. Each subject has 80 folders in visible, depth, and thermal domains for pain level recognition tasks.	Med.& Sci.	

Table 4		continued...							
MS Focus [127]		building, car, corridor, head, keyboard, office desk, pens	420	640x480	Canon EOS 350D FLIR SC660	8 HE	(<i>pub</i>) Contains 420 images of 7 objects in different optical focus positions, captured in visible, near-infrared, and thermal spectrum.	Industrial	
MM-Bio [23]		face	2500	not specified	FLIR E40	8 HE	(<i>rr</i>) A multi-modal biometric dataset containing thermal and RGB images of 125 people.	Mil. & Sur.	
MM-Hand [1]		hand	65K	412x273	not specified	8 HE	(<i>pub</i>) Multi-modal Hand Gesture Recognition dataset presents near-infrared images of 15 different hand gestures from 15 different subjects (5 women and 10 men).	Scientific	
Mov-Tar [106]		vegetation, building	150K	640x512	not specified	8 HE	(<i>pub</i>) This dataset contains synthetic small infrared targets embedded in IR background images to be used for target detection and tracking applications.	Mil. & Sur.	
MS-SS [43]		car, person, bike	1569	480x640	InfReC R500	8* HE	(<i>pub</i>) Contains RGB-Thermal combined images of autonomous vehicles with pixel-level annotations.	Industrial	
MSSpoof [21]		face	4.5K	1280x1024	uEye camera	8 HE	(<i>rr</i>) The dataset contains visible and NIR face images of 21 subjects, designed for spoofing attacks. It provides manual face annotations with 16 key point coordinates.	Mil. & Sur.	
MS-OD [55]		bike, car, person	30K	320x256 640x480	InfReC R500 InfReC H8000 Xeva-1.7-320	8 HE	(<i>pub</i>) The Multi-Spectral Object Detection dataset contains RGB, NIR, MIR and FIR images for automatic mobile robot tasks in traffic. The authors also present the ground truth labels. There are 7512 images per domain.	Industrial	
Multi-Focus [11]		uncategorised	576	320x240	TESTO 882-3	8 HE	(<i>rr</i>) The set consists of six image sets acquired at different lens positions, by manually moving the lens in 1 mm steps. Each set consists of 96 different images of a single scene.	Industrial	
ND X1 [20]		face	4584	not specified	Merlin uncooled μ -bol.	8 HE	(<i>rr</i>) The set includes 2292 IR and 2292 visible face images from 82 subjects.	Mil. & Sur.	
ND-NIVL [13]		face	25K	4770x3177 4288x2848	Nikon D90 Canon EOS 50D	8 HE	(<i>rr</i>) The dataset includes RGB face images obtained from 574 subjects and NIR face images obtained from 230 subjects. There are 2341 frames in the visible domain and 22264 frames in the IR domain.	Mil. & Sur.	
NOAA [94]		animal	80K	640x512	FLIR A6751 SLS	14 RAW	(<i>pub</i>) Contains visible and IR aerial images with annotations. There are additional images with no objects/animals. It can be used for detecting animals on sea ice.	Scientific	

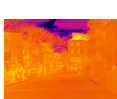
Table 4	continued...							
NTU RGB+D [97]		120 human actions	114K	512x424	Kinect V2	8 HE	(<i>rr</i>) The dataset contains RGB videos, depth map sequences, 3D skeletal data, and infrared (IR) videos of 82 daily actions, 12 medical conditions, and 26 mutual actions.	Scientific
OSU-CTD [29]		vehicle, pedestrian	17089	320x240	Raytheon PalmIR 250D	8* HE	(<i>pub</i>) The OSU Color-Thermal Database (CTD) includes six colour/thermal sequences, collected at three locations, used for fusion and fusion-based object detection in colour or thermal imagery.	Mil. & Sur.
OSU TPD [28]		pedestrian	284	360x240	Raytheon 300D	8 HE	(<i>pub</i>) The OSU Thermal Pedestrian Database (TPD) includes 10 sequences of videos with annotations of pedestrians who are 50% visible in images.	Mil. & Sur.
OTCBVS-P [15]		pedestrian	5390	480x360	FLIR A40M	8* HE	(<i>pub</i>) Pedestrian Infrared/visible Stereo Video dataset contains 4 visible and infrared video sequences of several people walking with 206 annotated frames and 25819 ground-truth point pairs.	Mil. & Sur.
Overhead [112]		pedestrian	1.9K	640x370	FLIR Vue T220	8* HE	(<i>pub</i>) The dataset presents thermal images from a UAV perspective, with object annotations. The images do not always include objects.	Mil. & Sur.
Parma [14]		pedestrian	18K	320x240	not specified	not specified	(<i>pri</i>) Parma Tetravision dataset, includes visible and infrared images captured from a car, with pedestrian annotations.	Mil. & Sur.
PETS 2005 [104]		vehicle	5K	320x256	not specified	8* HE	(<i>pub</i>) This an aerial vehicle tracking dataset containing 6 visible and 3 thermal infrared video sequences with annotations.	Mil. & Sur.
PTB-TIR [66]		vehicle, pedestrian	30128	up to 1280x720	8 dif. cams.	8 HE	(<i>pub</i>) TIR pedestrian tracking dataset include manually annotated 60 thermal sequences, divided into nine subsets with different shooting properties. The images are captured indoor and outdoor environments with surveillance, hand-held, vehicle-mounted and drone cameras during day and night.	Mil. & Sur.
RGB-NIR [18]		building, mountain, tree, car, motorcycle, etc.	477	1024x768	Canon T1i	8* HE	(<i>pub</i>) The dataset contains RGB and NIR images of 9 categories: country, field, forest, indoor, mountain, old buildings, street, urban, and water. Some frames include objects like buildings, trees, cars and motorcycles.	Scientific
RGBT Salient [111]		various objects	5000	640x480	FLIR T640 T610	8 HE	(<i>pub</i>) This dataset contains 5000 thermal/RGB image pairs with ground truth annotations of various objects like sneakers, pontoon, stool, dustbin, headphones for salient object detection tasks.	Scientific
RIFIR [71]		pedestrian	20K	640x480	not specified	8* HE	(<i>pub</i>) The dataset contains sequences of images, captured in an urban environment with one FIR and two colour cameras. There are train and test sets, with annotated pedestrians in both visible and IR domains.	Mil. & Sur.

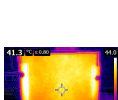
Table 4		continued...						
Roboflow-P [86]		person	13K	640x512	not specified	8* HE	(<i>pub</i>) The dataset contains IR images of people with annotations. Augmented images are also available.	Mil. & Sur.
SAGEM [26]		vehicle, etc.	1400	384x256	MWIR Matis	16 RAW	(<i>rr</i>) The dataset contains 16bits raw IR aerial images of vehicles for classification and detection tasks.	Mil. & Sur.
SCUT-FIR [121]		pedestrian	211K	720x576	NV628	8 HE	(<i>pub</i>) The dataset consists of approximately 11-hour-long image sequences captured in various traffic scenarios. 11 road segments are captured in different environments, such as the city centre, suburbs, highway, and campus.	Mil. & Sur.
SDT [105]		person	48K	640x480	FLIR Lepton 3.5	16 RAW	(<i>pub</i>) The dataset includes 40k synthetic and 8k real depth and thermal stereo images for human behaviour recognition and person detection tasks, with bounding box annotations.	Mil. & Sur.
SENSIAC [96]		people, vehicles, etc	not publicly specified	not publicly specified	not publicly specified	not publicly specified	(<i>pri</i>) The dataset contains 207 GB of videos in the IR domain and 106 GB of videos in the visible domain with ground truth data for automatic target recognition (ATR) tasks. Collected by the US Army Night Vision and Electronic Sensors Directorate (NVESD).	Mil. & Sur.
Server [65]		server hardware	1351	320x240	FLIR E8	8* HE	(<i>pub</i>) The dataset contains thermal images of servers for detecting the overheated area of the server surface, with five categories: normal status, main fan failure, vice-fan failure, air vent blockage and low-load status.	Industrial
SG-Ship [85]		ship	24K	1080x1920	Canon 70D	8* HE	(<i>pub</i>) Singapore Maritime dataset The ship videos, are captured at various locations around Singapore waters. The set is divided into three parts, 40 videos for visible on-shore, 11 videos for visible on-board and 30 videos for NIR on-shore shots. The dataset provides annotations in .mat format in 3 folders: horizon, object and track.	Mil. & Sur.
Soccer [35]		people	3000	1920x480	AXIS Q1922	8 HE	(<i>pub</i>) The dataset provides four thermal infrared video sequences of eight soccer players at an indoor sports arena.	Mil. & Sur.
Spindle [120]		lathe milling	1500	640x480	not specified	8* HE	(<i>rr</i>) Spindle thermal error prediction dataset contains all the thermal images and error data of a spindle, taken on a lathe and a milling machine.	Industrial
Surf-Coat [99]		various materials	449	320x240	FLIR E4	8* HE	(<i>pub</i>) This dataset contains raw temperature measurement data of external, and internal surfaces and air in the interior of a structure under different conditions. It has also surface thermographic images of different types of coatings and diffuses reflectance data for these materials.	Industrial

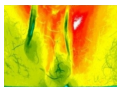
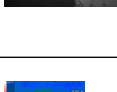
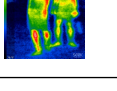
Table 4		continued...						
Terravic-F [70]		face	23K	320x240	Raytheon L3	8 HE	(<i>pub</i>) The Terravic Facial dataset consists of 20 thermal infrared facial image sequences, captured from the front, left and right at indoor and outdoor environments.	Mil. & Sur.
Terravic-M [70]		human, plane, dock	22K	320x240	Raytheon L3	8 HE	(<i>pub</i>) The Terravic Motion dataset has 18 sequences of thermal infrared images, captured at indoor and outdoor environments for object detection and tracking tasks.	Mil. & Sur.
Terravic-W [70]		person, weapon	3555	320x240	Raytheon L3	8 HE	(<i>pub</i>) The dataset includes 5 thermal IR image sequences for weapon detection and weapon evacuation detection tasks.	Mil. & Sur.
TestisT [40]		testis	50	640x320	VIS-IR 640	8 HE	(<i>pub</i>) The Testis Thermography dataset contains 50 thermal testis images to detect varicocele.	Medical
THALES [26]		vehicle, boat	more than 6K	320x240 640x512	not specified	8/16 HE/RAW	(<i>rr</i>) Contains aerial images obtained from six hours of video recorded from a helicopter in different environments, such as urban, expressway, rural, etc.	Mil. & Sur.
The Flame [98]		fire	49K	640x512 3840x2160	FLIR Vue Pro R DJI Phantom 3	8* HE	(<i>rr</i>) The dataset consists of raw aerial video and raw heat map footage captured by drones, during a pile burn in Northern Arizona. Collected for wildfire detection and includes 47992 labelled frames for fire classification and 2003 ground truth masked frames for fire segmentation.	Mil. & Sur.
TIDOC [7]		car, cat, pedestrian	6892	300x400 1080x1440	FLIR Seek Thermal	8* HE	(<i>pub</i>) The Thermal Image dataset for Object Classification (TIDOC) includes thermal images of three classes, car, cat, and pedestrian.	Mil. & Sur.
TI Mo [93]		person	635.6K	512x512 288x320	Microsoft Azure Kinect RGB-D	16 RAW	(<i>rr</i>) The time-of-Flight Indoor Monitoring dataset presents IR and depth videos. Totally, 612 K frames for anomaly detection and 23.6 K frames for person detection, with annotations for both tasks. For person detection, bounding boxes and segmentation masks are available.	Mil. & Sur.
TIRDRD [123]		road	6000	640x480	FLIR A655SC	8 HE	(<i>pub</i>) Thermal IR-based Drivable Region Detection dataset consists of about 6000 manually annotated images, with road scenarios, such as on-road, off-road, and cluttered road for drivable region detection tasks.	Mil. & Sur.
TNO [109]		objects, person, vehicle	400	256x256	Amber Radiance 1	8* HE	(<i>pub</i>) The TNO Image Fusion Dataset consists of visual and IR pairs of images captured at night time.	Mil. & Sur.
Transformer [75]		transformer, induction motors	255	320x240	Dali-tech T4/T8	8* HE	(<i>pub</i>) The dataset contains thermal images of induction motors and transformers for the purpose of condition monitoring.	Industrial

Table 4		continued...						
TRICLOBS [110]		people, vehicle	57K	640x480	XenIC's Gobi 384	8 HE	(<i>pub</i>) The TRICLOBS (TRI-band Color Low Light OBServation) dataset contains video sequences in visible, NIR and LWIR bands. The main purpose of this dataset is to use image fusion and colour-mapping algorithms for surveillance applications.	Mil. & Sur.
Tufts-Face [79]		face	100K	not specified	various cameras	not specified	(<i>rr</i>) Tufts-Face-Database has more than 100K face images of 7 image modes: visible, NIR, thermal, computerised sketch, video, plenoptic and 3D images.	Mil. & Sur.
UL-FMTV [41]		face	71400	640x512	Indigo Phoenix Thermal	8 HE	(<i>rr</i>) The ULFMT video dataset includes MWIR band facial videos of 238 subjects for facial pose and expression recognition applications.	Mil. & Sur.
UNIRI-TID [60]		person	11K	1280x960	FLIR Therma -Cam P10	8 HE	(<i>rr</i>) This is a collection of thermal videos and images that simulate illegal border crossings and movements in protected areas. The videos were shot in and around the forest at night and in various weather conditions.	Mil. & Sur.
VAIS [126]		ship	1242	1024x680	Sofradir EC Atom 1024	8 HE	(<i>pub</i>) VAIS includes IR and visible image sequences of actual ship images captured from piers, along with annotations.	Mil. & Sur.
Valle-Aerial [37]		road, car	110	336x256	Zemuse XT	8* HE	(<i>pub</i>) The dataset is made up of thermal and visible aerial images of a planar scene captured using a UAV at Universidad del Valle in Cali, Colombia.	Mil. & Sur.
VAP [78]		people	11537	640x480	AXIS Q1922	16/32 HE/RAW	(<i>pub</i>) The dataset contains RGB (32bit), depth (16bit), and thermal (32bit) images of people for human detection, human segmentation, person re-identification tasks, with 5724 annotated frames.	Mil. & Sur.
ViViD++ [63]		uncate- gorised	9290	640x480	FLIR A65	8 HE	(<i>rr</i>) The dataset provides normal and poor illumination sequences, captured by thermal, depth, and temporal difference sensors for indoor and outdoor environments.	Scientific
VOT-RGBTIR [59]		pedestrian, bike, car, dog, motorcycle	20K	around 600x400	not specified	8* HE	(<i>pub</i>) VOT-RGB TIR 2019 dataset includes infrared images in 60 sequences. Each sequence contains various numbers of images with objects like cars, pedestrians, motorcycles, etc. The dataset has different object annotations, such as baby, child or cars with colour, etc.	Mil. & Sur.

[4] Alqattan M (2020) A dataset of raw thermal, visible and night vision images for illegal fishers in the kuwaiti bay. <https://doi.org/10.17632/69ncy4nxsg.1>, Available at <https://data.mendeley.com/datasets/69ncy4nxsg/1>

[5] Aniket A (2022) bird dataset. Available at <https://universe.roboflow.com/antiuav-9-aniket/bird-6le8u>

[6] Ariffin SMZSZ, Jamil N, Rahman PNMA (2016) Diast variability illuminated thermal

- and visible ear images datasets. In: 2016 Signal Processing: Algorithms, Architectures, Arrangements, and Applications (SPA), pp 191–195, <https://doi.org/10.1109/SPA.2016.7763611>, Available at <http://vcipl-okstate.org/pbvs/bench/>
- [7] Ashfaq Q, Akram U, Zafar R (2021) Thermal image dataset for object classification. <https://doi.org/10.17632/btmrycjbj.1>, Available at <https://data.mendeley.com/datasets/btmrycjbj/1>
- [8] AV-Public (2022) All thermal dataset. Available at https://universe.roboflow.com/avpublic/all_ther
- [9] Bagavathiappan S, Lahiri B, Saravanan T, et al (2013) Infrared thermography for condition monitoring - a review. *Infrared Physics and Technology* 60:35–55
- [10] Bahnsen CH, Moeslund TB (2018) Rain removal in traffic surveillance: Does it matter? *IEEE Transactions on Intelligent Transportation Systems* pp 1–18. <https://doi.org/10.1109/TITS.2018.2872502>, Available at <https://www.kaggle.com/aalborguniversity/aau-rainsnow/>
- [11] Benes R, Dvorak P, Faundez-Zanuy M, et al (2013) Multi-focus thermal image fusion. *Pattern Recognition Letters* 34(5):536–544. Available at <http://splab.cz/en/download/databaze/multi-focus-thermal-image-database>
- [12] Berg A, Ahlberg J, Felsberg M (2015) A thermal object tracking benchmark. In: *Advanced Video and Signal Based Surveillance (AVSS)*, 2015 12th IEEE International Conference on, Available at <http://www.cvl.isy.liu.se/en/research/datasets/ltir/version1.0/>
- [13] Bernhard J, Barr J, Bowyer KW, et al (2015) Near-ir to visible light face matching: Effectiveness of pre-processing options for commercial matchers. In: 2015 IEEE 7th International Conference on Biometrics Theory, Applications and Systems (BTAS), pp 1–8, <https://doi.org/10.1109/BTAS.2015.7358780>, Available at <https://cvrl.nd.edu/projects/data/>
- [14] Bertozzi M, Broggi MVGDRMA and Felisa (2006) Low-level pedestrian detection by means of visible and far infra-red tetra-vision. Maintained by <http://vislab.it/>
- [15] Bilodeau GA, Torabi A, St-Charles PL, et al (2014) Thermal-visible registration of human silhouettes: A similarity measure performance evaluation. *Infrared Physics and Technology* 64:79–86. Available at <http://vcipl-okstate.org/pbvs/bench/>
- [16] Bondi E, Jain R, Aggrawal P, et al (2020) Birdsai: A dataset for detection and tracking in aerial thermal infrared videos. In: *WACV*, Available at <https://sites.google.com/view/elizabethbondi/dataset>
- [17] Boreman GD (1998) *Basic electro-optics for electrical engineers*, vol 31. SPIE Press
- [18] Brown M, Süsstrunk S (2011) Multispectral SIFT for scene category recognition. In: *Computer Vision and Pattern Recognition (CVPR11)*, Colorado Springs, pp 177–184, Available at https://ivrlwww.epfl.ch/supplementary_material/cvpr11/index.html
- [19] Buser RG, Tompsett MF (1997) Historical overview. In: *Semiconductors and Semimetals*, vol 47. Elsevier, p 1–16
- [20] Chen X, Flynn P, Bowyer K (2005) Ir and visible light face recognition. *Computer Vision and Image Understanding* 99:332–358. <https://doi.org/10.1016/j.cviu.2005.03.001>, Available at <https://cvrl.nd.edu/projects/data/>
- [21] Chingovska I, Erdogmus N, Anjos A, et al (2016) *Face Recognition Systems Under Spoofing Attacks*, Springer International Publishing, Cham, pp 165–194. https://doi.org/10.1007/978-3-319-28501-6_8, URL https://doi.org/10.1007/978-3-319-28501-6_8, Available at <https://www.idiap.ch/en/dataset/msspoof>

- [22] Clerke AM (2003) A popular history of astronomy during the nineteenth century. Sattre Pr
- [23] Computer Vision and Biometrics Lab. (2022) Multimodal biometrics dataset thermal face images. Available at <https://cvbl.iitit.ac.in/dataset.php>
- [24] Cosar S, Bellotto N (2019) Human re-identification with a robot thermal camera using entropy-based sampling. Journal of Intelligent and Robotic Systems <https://doi.org/https://doi.org/10.1007/s10846-019-01026-w>, Available at <https://lcas.lincoln.ac.uk/wp/research/data-sets-software/l-cas-rgb-d-t-re-identification-dataset/>
- [25] Coşar S, Yan Z, Zhao F, et al (2018) Thermal camera based physiological monitoring with an assistive robot. In: 2018 40th Annual International Conference of the IEEE Engineering in Medicine and Biology Society (EMBC), pp 5010–5013, <https://doi.org/10.1109/EMBC.2018.8513201>, Available at <https://lcas.lincoln.ac.uk/wp/research/data-sets-software/>
- [26] D’Angelo E, Herbin S, Ratieville M (2006) Robin challenge. Available at <https://robin.inrialpes.fr/testdefinitions.php>
- [27] Daniels A (2018) Field Guide to Infrared Optics, Materials, and Radiometry, vol FG39. SPIE
- [28] Davis JW, Keck MA (2005) A two-stage template approach to person detection in thermal imagery. In: 2005 Seventh IEEE Workshops on Applications of Computer Vision (WACV/MOTION’05)-Volume 1, IEEE, pp 364–369, Available at <http://vcipl-okstate.org/pbvs/bench/>
- [29] Davis JW, Sharma V (2007) Background-subtraction using contour-based fusion of thermal and visible imagery. Computer vision and image understanding 106(2-3):162–182. Available at <http://vcipl-okstate.org/pbvs/bench/>
- [30] Dodge SF, Karam LJ (2017) A study and comparison of human and deep learning recognition performance under visual distortions. CoRR abs/1705.02498. URL <http://arxiv.org/abs/1705.02498>, <https://arxiv.org/abs/1705.02498>
- [31] Erazo-Aux J, Loaiza-Correa H, Restrepo-Giron AD, et al (2020) Thermal imaging dataset from composite material academic samples inspected by pulsed thermography. Data in brief 32:106,313. <https://doi.org/10.1016/j.dib.2020.106313>, URL <https://europepmc.org/articles/PMC7508994>, Available at <https://data.mendeley.com/datasets/v4knrwgj9y/2>
- [32] Faundez-Zanuy M, Mekyska J, Espinosa-Duró V (2011) On the focusing of thermal images. Pattern Recognition Letters 32:1548–1557. <https://doi.org/10.1016/j.patrec.2011.04.022>, Available at <http://splab.cz/en/download/database/thermal-focus-image-database>
- [33] Faundez-Zanuy M, Mekyska J, Font X (2013) A new hand image database simultaneously acquired in visible, near-infrared and thermal spectrums. Cognitive Computation 6. <https://doi.org/10.1007/s12559-013-9230-3>, Available at <http://splab.cz/en/download/database/carl-database>
- [34] FLIR (2022) Free flir thermal dataset for algorithm training. Available at <https://www.flir.com/oem/adas/adas-dataset-form/>
- [35] Gade R, Moeslund TB (2018) Constrained multi-target tracking for team sports activities. IPSJ Transactions on Computer Vision and Applications 10(1):1–11. Available at <https://www.kaggle.com/aalborguniversity/thermal-soccer-dataset>
- [36] Gao C, Du Y, Liu J, et al (2016) Infrared dataset: Infrared action recognition at different times. Neurocomputing 212:36–47. <https://doi.org/https://doi.org/10.1016/j.neucom.2016.05.094>, Available at <https://drive.google.com/file/d/0B8URzo24xEIURU1Oa0ctYmpaTk/view?>

usp = sharing & resourcekey = 0-6EOSjRX7_Ea-14tJorumrg

- [37] Garcia L, Diaz J, Loaiza Correa H, et al (2020) Thermal and visible aerial imagery. <https://doi.org/10.17632/ffgxxzx298.2>, Available at <https://data.mendeley.com/datasets/ffgxxzx298/2>
- [38] Gebhardt E, Wolf M (2018) Camel dataset for visual and thermal infrared multiple object detection and tracking. In: 2018 15th IEEE International Conference on Advanced Video and Signal Based Surveillance (AVSS), IEEE, pp 1–6, Available at <https://camel.ece.gatech.edu/>
- [39] Ghayoumi zadeh H, Haddadnia J, Seryasat O, et al (2016) Segmenting breast cancerous regions in thermal images using fuzzy active contours <https://doi.org/10.17877/DE290R-17666>, Available at <http://database.irthermo.ir/>
- [40] Ghayoumi zadeh H, Namdari F, Dadpay M, et al (2017) Evaluation of thermal imaging in the diagnosis and classification of varicocele. Iranian journal of medical physics 14:114–121. <https://doi.org/10.22038/ijmp.2017.20753.1200>, Available at <http://database.irthermo.ir/>
- [41] Ghiass R, Bendada H, Maldague X (2018) Université laval face motion and time-lapse video database (ul-fmtv). <https://doi.org/10.21611/qirt.2018.051>, Available at <http://www.qirt.org/liens/FMTV.htm>
- [42] Gonzalez Alzate A, Fang Z, Socarras Y, et al (2016) Pedestrian detection at day/night time with visible and fir cameras: A comparison. Sensors 16:820. <https://doi.org/10.3390/s16060820>
- [43] Ha Q, Watanabe K, Karasawa T, et al (2017) Mfnet: Towards real-time semantic segmentation for autonomous vehicles with multispectral scenes. In: 2017 IEEE/RSJ International Conference on Intelligent Robots and Systems (IROS), pp 5108–5115, <https://doi.org/10.1109/IROS.2017.8206396>, Available at https://www.mi.t.u-tokyo.ac.jp/static/projects/mil_multispectral/
- [44] HACARUS Inc. (2020) Near infrared hyperspectral image dataset. Available at <https://www.kaggle.com/hacarus/near-infrared-hyperspectral-image>
- [45] HAMAMATSU PHOTONICS K.K., Solid State Division (2011) Characteristics and Use of Infrared Detectors. Tech. rep.
- [46] Haque MA, Bautista RB, Noroozi F, et al (2018) Deep multimodal pain recognition: a database and comparison of spatio-temporal visual modalities. In: 2018 13th IEEE International Conference on Automatic Face and Gesture Recognition (FG 2018), IEEE, pp 250–257, Available at <https://vap.aau.dk/mintpain-database/>
- [47] He Y, Deng B, Wang H, et al (2021) Infrared machine vision and infrared thermography with deep learning: A review. Infrared physics and technology 116
- [48] Hou F, Zhang Y, Zhou Y, et al (2022) Review on infrared imaging technology. Sustainability 14(18). <https://doi.org/10.3390/su141811161>, URL <https://www.mdpi.com/2071-1050/14/18/11161>
- [49] Huda NU, Hansen BD, Gade R, et al (2020) The effect of a diverse dataset for transfer learning in thermal person detection. Sensors 20(7). Available at <https://www.kaggle.com/noorulhuda90/aaupdt>
- [50] Hudson R, Hudson J, Levinstein H (1976) Infrared detectors. Physics Today 29(3):59
- [51] Hui B, Song Z, Fan H, et al (2019) A dataset for infrared image dim-small aircraft target detection and tracking under ground / air background. <https://doi.org/doi:10.11922/sciencedb.902>, URL <http://www.dx.doi.org/10.11922/sciencedb.902>, Available at [https://www.scidb.cn/en/detail?dataSetId=720626420933459968 & dataSetType=journal](https://www.scidb.cn/en/detail?dataSetId=720626420933459968&dataSetType=journal)
- [52] Hwang S, Park J, Kim N, et al (2015) Multispectral pedestrian detection: Benchmark

- dataset and baseline. In: Proceedings of the IEEE conference on computer vision and pattern recognition, pp 1037–1045, Available at <https://soonminhwang.github.io/rgb-t-ped-detection/>
- [53] Iwashita Y, Nakashima K, Stoica A, et al (2019) Tu-net and tdeeplab: Deep learning-based terrain classification robust to illumination changes, combining visible and thermal imagery. pp 280–285, <https://doi.org/10.1109/MIPR.2019.00057>, Available at http://robotics.ait.kyushu-u.ac.jp/~yumi/db/jpl_marsyard_db.html
- [54] Jia X, Zhu C, Li M, et al (2021) Llvip: A visible-infrared paired dataset for low-light vision. In: Proceedings of the IEEE/CVF International Conference on Computer Vision, pp 3496–3504, Available at <https://bupt-ai-cz.github.io/LLVIP/>
- [55] Karasawa T, Watanabe K, Ha Q, et al (2017) Multispectral object detection for autonomous vehicles. Proceedings of the on Thematic Workshops of ACM Multimedia 2017 Available at https://www.mi.t.u-tokyo.ac.jp/static/projects/mil_multispectral/
- [56] Karim A, Andersson JY (2013) Infrared detectors: Advances, challenges and new technologies. In: IOP Conference Series: Materials Science and Engineering, IOP Publishing, p 012001
- [57] Kong S, Heo J, Boughorbel F, et al (2007) Multiscale fusion of visible and thermal ir images for illumination-invariant face recognition. International Journal of Computer Vision 71:215–233. <https://doi.org/10.1007/s11263-006-6655-0>, Available at <http://vcipl-okstate.org/pbvs/bench/>
- [58] Korki14 (2022) Drones dataset. Available at <https://universe.roboflow.com/korki14/drones-srdze>
- [59] Kristan M, Matas J, Leonardis A, et al (2016) A novel performance evaluation methodology for single-target trackers. IEEE Transactions on Pattern Analysis and Machine Intelligence 38(11):2137–2155. <https://doi.org/10.1109/TPAMI.2016.2516982>, Available at <https://www.votchallenge.net/vot2019/dataset.html>
- [60] Krišto M, Ivasic-Kos M, Pobar M (2020) Thermal object detection in difficult weather conditions using yolo. IEEE Access 8:125,459–125,476. <https://doi.org/10.1109/ACCESS.2020.3007481>, Available at <https://dx.doi.org/10.21227/yec9-yy29>
- [61] Kruse P (1995) A comparison of the limits to the performance of thermal and photon detector imaging arrays. Infrared Physics and Technology 36(5):869–882. [https://doi.org/https://doi.org/10.1016/1350-4495\(95\)00014-P](https://doi.org/https://doi.org/10.1016/1350-4495(95)00014-P), URL <https://www.sciencedirect.com/science/article/pii/S135044959500014P>
- [62] Kumar A, Srikanth T (2008) Online personal identification in night using multiple face representations. In: 2008 19th International Conference on Pattern Recognition, pp 1–4, <https://doi.org/10.1109/ICPR.2008.4761695>, Available at <https://www4.comp.polyu.edu.hk/~csajaykr/IITD/FaceIR.htm>
- [63] Lee AJ, Cho Y, Shin Ys, et al (2019) Vivid : Vision for visibility dataset. Available at <https://visibilitydataset.github.io/>
- [64] Li SZ, Chu R, Liao S, et al (2007) Illumination invariant face recognition using near-infrared images. IEEE Transactions on pattern analysis and machine intelligence 29(4):627–639. Available at <http://vcipl-okstate.org/pbvs/bench/>
- [65] Liu H, Bao C, Xie T, et al (2019) Research on the intelligent diagnosis method of the server based on thermal image technology. Infrared Physics and Technology 96:390–396. Available at <https://www.kaggle.com/liuhangaz/thermal-images-of-the-server>
- [66] Liu Q, He Z (2018) PTB-TIR: A thermal infrared pedestrian tracking benchmark. CoRR abs/1801.05944. URL <http://arxiv.org/abs/1801.05944>, Available at https://github.com/QiaoLiuHit/PTB-TIR_Evaluation_toolkit, <https://arxiv.org/abs/1801.05944>

- [67] Liu Q, Li X, He Z, et al (2020) Lsotb-tir: A large-scale high-diversity thermal infrared object tracking benchmark. <https://doi.org/10.1145/3394171.3413922>, Available at <https://github.com/QiaoLiuHit/LSOTB-TIR>
- [68] Lord SD (1992) A new software tool for computing Earth's atmospheric transmission of near- and far-infrared radiation. NASA Technical Memorandum 103957
- [69] Mantecon T, Del-Blanco C, Jaureguizar F, et al (2016) Hand gesture recognition using infrared imagery provided by leap motion controller. pp 47–57, https://doi.org/10.1007/978-3-319-48680-2_5, Available at <https://www.kaggle.com/gti-upm/leapgestrecog>
- [70] Mieziako R (accessed on 2022) Terravic research infrared database. Available at <http://vcipl-okstate.org/pbus/bench/>
- [71] Miron A (2014) Multi-modal, multi-domain pedestrian detection and classification : Proposals and explorations in visible over stereovision, fir and swir Available at <https://zenodo.org/record/3754168#.YIvye7UzZPa>
- [72] Mohd Asaari MS, Suandi SA, Rosdi B (2014) Fusion of band limited phase only correlation and width centroid contour distance for finger based biometrics. Expert Systems with Applications 41:3367–3382. <https://doi.org/10.1016/j.eswa.2013.11.033>, Available at http://drfendi.com/fv_usm_database/
- [73] Morris N, Avidan S, Matusik W, et al (2007) Statistics of infrared images. pp 1–7, <https://doi.org/10.1109/CVPR.2007.383003>, Available at <http://www.dgp.toronto.edu/~nmorris/IR/>
- [74] Naik S (2019) Thermal mango image dataset - flir one. <https://doi.org/10.17632/vksfkmphzs.1>, Available at <https://data.mendeley.com/datasets/vksfkmphzs/1>
- [75] Najafi M, Baleghi Y, Mirimani SM (2021) Thermal images dataset, transformer, 1 phase dry type. <https://doi.org/10.17632/8mg8mkc7k5.2>, Available at <https://data.mendeley.com/datasets/8mg8mkc7k5/2>
- [76] Nelson J (2020) Thermal dogs and people object detection dataset. Available at <https://public.roboflow.com/object-detection/thermal-dogs-and-people>
- [77] Olmeda D, Premebida C, Nunes U, et al (2013) Pedestrian detection in far infrared images. Integrated Computer-Aided Engineering 20. <https://doi.org/10.3233/ICA-130441>, Available at <https://e-archivo.uc3m.es/handle/10016/17370>
- [78] Palmero C, Clapés A, Holmberg Bahnsen C, et al (2016) Multi-modal rgb–depth–thermal human body segmentation. International Journal of Computer Vision 118. <https://doi.org/10.1007/s11263-016-0901-x>, Available at <https://vap.aau.dk/vap-trimodal-people-segmentation-dataset/>
- [79] Panetta K, Wan Q, Agaian S, et al (2018) A comprehensive database for benchmarking imaging systems. IEEE transactions on pattern analysis and machine intelligence 42(3):509–520. Available at https://www.kaggle.com/kpvisionlab/tufts-face-database?select=file_1
- [80] Parr AC, Datla R, Gardner J (2005) Optical radiometry, vol 41. Elsevier
- [81] Patino L, Cane T, Vallee A, et al (2016) Pets 2016: Dataset and challenge. In: Proceedings of the IEEE Conference on Computer Vision and Pattern Recognition Workshops, pp 1–8, Available at <http://www.cvg.reading.ac.uk/PETS2016/a.html>
- [82] Perpetuini D, Filippini C, Cardone D, et al (2021) An overview of thermal infrared Imaging-Based screenings during pandemic emergencies. International Journal of Environmental Research and Public Health 18(6)
- [83] Piñeiro-Ave J, Blanco-Velasco M, Cruz-Roldán F, et al (2014) Target detection for low cost uncooled mwir cameras based on empirical mode decomposition. Infrared Physics and Technology 63:222–231

- [84] Portmann J, Lynen S, Chli M, et al (2014) People detection and tracking from aerial thermal views. In: 2014 IEEE International Conference on Robotics and Automation (ICRA), pp 1794–1800, <https://doi.org/10.1109/ICRA.2014.6907094>, Available at <https://projects.asl.ethz.ch/datasets/doku.php?id=ir%3Airicra2014>
- [85] Prasad DK, Rajan D, Rachmawati L, et al (2017) Video processing from electro-optical sensors for object detection and tracking in a maritime environment: A survey. IEEE Transactions on Intelligent Transportation Systems 18(8):1993–2016. <https://doi.org/10.1109/TITS.2016.2634580>, Available at <https://sites.google.com/site/dilipprasad/home/singapore-maritime-dataset>
- [86] Projects RU (2022) People detection - thermal dataset. Available at <https://universe.roboflow.com/roboflow-universe-projects/people-detection-thermal>
- [87] Rivadeneira RE, Suárez PL, Sappa AD, et al (2019) Thermal image superresolution through deep convolutional neural network. In: International Conference on Image Analysis and Recognition, Springer, pp 417–426, Available at <https://github.com/rafariva/ThermalDatasets>
- [88] Rivadeneira RE, Sappa AD, Vintimilla BX (2020) Thermal image super-resolution: a novel architecture and dataset. In: International Conference on Computer Vision Theory and Applications, pp 1–2, Available at <https://github.com/rafariva/ThermalDatasets>
- [89] Roboflow (2020) Thermal cheetah object detection dataset. Available at <https://public.roboflow.com/object-detection/thermal-cheetah>
- [90] Rogalski A (1997) Infrared thermal detectors versus photon detectors: I. Pixel performance. In: Sizov FF, Tetyorkin VV (eds) Material Science and Material Properties for Infrared Optoelectronics, International Society for Optics and Photonics, vol 3182. SPIE, pp 14–25, URL <https://doi.org/10.1117/12.280417>
- [91] Rogalski A (2002) Infrared detectors: an overview. Infrared physics and technology 43(3-5):187–210
- [92] S. Pini GBRVA, D'Eusania, Cucchiara R (2020) Baracca: a multimodal dataset for anthropometric measurements in automotive. In: Proceedings of the International joint Conference on Biometrics (IJCB), Available at <https://aimagelab.ing.unimore.it/imagelab/page.asp?IdPage=37>
- [93] Schneider P, Anisimov Y, Islam R, et al (2022) Timo: a dataset for indoor building monitoring with a time-of-flight camera. Sensors 22(11). <https://doi.org/10.3390/s22113992>, URL <https://www.mdpi.com/1424-8220/22/11/3992>, Available at <https://vizta-tof.kl.dfki.de/timo-dataset-overview/>
- [94] Science Center AF (accessed on 2022) A dataset for machine learning algorithm development. Available at <https://lila.science/datasets/noaa-arctic-seals-2019/>
- [95] Sedik A, Abd El-Rahiem B, Abd El-Samie F, et al (2020) Mbd: Multi-biometric dataset. <https://doi.org/10.17632/94ksjgbwnz.1>, Available at <https://data.mendeley.com/datasets/94ksjgbwnz/1>
- [96] SENSIAC (2008) Military sensing information analysis center (sensiacy). Available at https://www.sensiac.org/external/products/list_databases/
- [97] Shahroudy A, Liu J, Ng TT, et al (2016) Ntu rgb+ d: A large scale dataset for 3d human activity analysis. In: Proceedings of the IEEE conference on computer vision and pattern recognition, pp 1010–1019, Available at <https://rose1.ntu.edu.sg/dataset/actionRecognition/>
- [98] Shamsoshoara A, Afghah F, Razi A, et al (2021) Aerial imagery pile burn detection using deep learning: The flame dataset. Computer Networks 193:108,001. <https://doi.org/10.1016/j.comnet.2021.108001>, Available at <https://dx.doi.org/10.21227/qad6-r683>

- [99] Silva A, Calado C (2020) Thermal and optical behavior dataset of surfaces coated with high reflectance and common materials under different conditions, used in brazil. Data in Brief 30:105,445. <https://doi.org/10.1016/j.dib.2020.105445>, Available at <https://data.mendeley.com/datasets/gnhjwsf6jf/2>
- [100] Socarras Y, Ramos S, Vazquez D, et al (2013) Adapting pedestrian detection from synthetic to far infrared images. Available at <http://adas.cvc.uab.es/elektra/enigma-portfolio/item-1/>
- [101] Soundrapandiyar R, Satapathy SC, P.V.S.S.R. CM, et al (2022) A comprehensive survey on image enhancement techniques with special emphasis on infrared images. Multimedia Tools and Applications 81(7):9045–9077. <https://doi.org/10.1007/s11042-021-11250-y>, URL <https://doi.org/10.1007/s11042-021-11250-y>
- [102] Sousa E, Vardasca R, Teixeira S, et al (2017) A review on the application of medical infrared thermal imaging in hands. Infrared Physics and Technology 85:315–323. <https://doi.org/https://doi.org/10.1016/j.infrared.2017.07.020>, URL <https://www.sciencedirect.com/science/article/pii/S1350449517304024>
- [103] Speth J, Vance N, Czajka A, et al (2021) Deception detection and remote physiological monitoring: A dataset and baseline experimental results Available at <https://cvrl.nd.edu/projects/data/>
- [104] Strat T (2005) Vivid tracking evaluation web site. Available at <http://vision.cse.psu.edu/data/vividEval/datasets/datasets.html>
- [105] Strohmayer J, Pramerdorfer C, Kampel M (2020) Sdt: A synthetic multi-modal dataset for person detection and pose classification Available at <https://zenodo.org/record/4124309#.YWlGKRpBxPZ>
- [106] Sun X, Guo L, Zhang W, et al (2021) A dataset for small infrared moving target detection under clutter background. v1. Available at <https://datapid.cn/31253.11>
- sciondb.j00001.00231
- [107] Teutsch M, Sappa AD, Hammoud RI (2021) Computer vision in the infrared spectrum: challenges and approaches. Synthesis Lectures on Computer Vision 10(2):1–138
- [108] Toet A (2002) Detection of dim point targets in cluttered maritime backgrounds through multisensor image fusion. In: Targets and Backgrounds VIII: Characterization and Representation, International Society for Optics and Photonics, pp 118–129, Available at https://figshare.com/articles/dataset/Kayak_image_fusion_sequence_Part_I/1007650
- [109] Toet A, IJspeert J, Waxman A, et al (1997) Fusion of visible and thermal imagery improves situational awareness. Displays 18(2):85–95. [https://doi.org/https://doi.org/10.1016/S0141-9382\(97\)00014-0](https://doi.org/https://doi.org/10.1016/S0141-9382(97)00014-0), Available at https://figshare.com/articles/dataset/TNO_Image_Fusion_Dataset/1008029?file=37872186
- [110] Toet A, Hogervorst MA, Pinkus AR (2016) The triclobs dynamic multi-band image dataset. Available at https://figshare.com/articles/dataset/The_TRICLOBS_Dynamic_Multiband_Image_Dataset/3206887/1
- [111] Tu Z, Ma Y, Li Z, et al (2020) Rgbt salient object detection: A large-scale dataset and benchmark. arXiv preprint arXiv:200703262 Available at <https://github.com/lz118/RGBT-Salient-Object-Detection>
- [112] UMDAMAV-Dataset (2022) Thermal overhead dataset. Available at https://universe.roboflow.com/umdamavdataset/thermal_overhead
- [113] Venkataraman B, Raj B (2003) Performance parameters for thermal imaging systems. Insight-Non-Destructive Testing and Condition Monitoring 45(8):531–535
- [114] Visual Lab. (accessed on 2022) Thermal images for breast cancer diagnosis dmr-ir. Available at <http://visual.ic.uff.br/en/>

proeng/thiagoelias/

- [115] Vollmer M, Möllmann KP (2017) Infrared thermal imaging: fundamentals, research and applications. John Wiley and Sons
- [116] Wang Y, Jodoin PM, Porikli F, et al (2014) Cdnet 2014: An expanded change detection benchmark dataset. In: Proceedings of the IEEE conference on computer vision and pattern recognition workshops, pp 387–394, Available at <http://jacarini.dinf.usherbrooke.ca/dataset2014/>
- [117] Wayne Treible SSAKMOBPKSCK-Philip Saponaro (2017) Cats: A color and thermal stereo benchmark. In: Conference on Computer Vision and Pattern Recognition (CVPR), Available at <http://bigdatavision.org/CATS/download.html>
- [118] Westlake ST, Volonakis TN, Jackman J, et al (2020) Deep learning for automatic target recognition with real and synthetic infrared maritime imagery. In: Artificial Intelligence and Machine Learning in Defense Applications II, International Society for Optics and Photonics, p 1154309, Available at <https://cord.cranfield.ac.uk/articles/dataset/IRShips/12800324>
- [119] Wu Z, Fuller N, Theriault D, et al (2014) A thermal infrared video benchmark for visual analysis. In: 2014 IEEE Conference on Computer Vision and Pattern Recognition Workshops, pp 201–208, <https://doi.org/10.1109/CVPRW.2014.39>, Available at <http://csr.bu.edu/BU-TIV/BUTIV.html>
- [120] Xiang S (2020) Spindle thermal error prediction approach based on thermal infrared images: a deep learning method. <https://doi.org/10.21227/vwp1-q708>, Available at <https://dx.doi.org/10.21227/vwp1-q708>
- [121] Xu Z, Zhuang J, Liu Q, et al (2019) Benchmarking a large-scale fir dataset for on-road pedestrian detection. Infrared Physics and Technology 96:199–208. <https://doi.org/https://doi.org/10.1016/j.infrared.2018.11.007>, Available at https://github.com/SCUT-CV/SCUT_FIR_Pedestrian_
- Dataset*
- [122] Yaman M, Kalkan S (2015) An iterative adaptive multi-modal stereo-vision method using mutual information Available at <https://kovan.ceng.metu.edu.tr/MMStereoDataset/>
- [123] Yoon JS, Park K, Hwang S, et al (2016) Thermal-infrared based drivable region detection. In: Intelligent Vehicles Symposium (IV), 2016 IEEE, IEEE, pp 978–985, Available at <https://sites.google.com/site/drivableregion/>
- [124] Zhang H, Luo C, Wang Q, et al (2018) A novel infrared video surveillance system using deep learning based techniques. Multimedia Tools and Applications 77(20):26,657–26,676. Available at <http://www.lpi.tel.uva.es/AALARTDATA>
- [125] Zhang L, Rui Y (2013) Image search—from thousands to billions in 20 years. ACM Trans Multimedia Comput Commun Appl 9(1s). <https://doi.org/10.1145/2490823>, URL <https://doi.org/10.1145/2490823>
- [126] Zhang MM, Choi J, Daniilidis K, et al (2015) Vais: A dataset for recognizing maritime imagery in the visible and infrared spectrums. In: 2015 IEEE Conference on Computer Vision and Pattern Recognition Workshops (CVPRW), pp 10–16, <https://doi.org/10.1109/CVPRW.2015.7301291>, Available at <http://vcip1-okstate.org/pbus/bench/>
- [127] Zukal M, Mekyska J, Cika P, et al (2013) Interest points as a focus measure in multi-spectral imaging. Radioengineering 22:68–81. Available at <http://splab.cz/en/download/databaze/multispec>

Appendix 1

4.1 List of Abbreviations

CT	Computerised Tomography
CTE	Coefficient of Thermal Expansion
D*	Detectivity
E	Emissivity
ES	Electromagnetic Spectrum
FHD	Full High Definition
FIR	Far-Infrared
FLIR	Forward Looking Infrared
FOV	Field-of-View
FPA	Focal Plane Array
HD	High Definition
HE	Histogram Equalization
IR	Infrared
LD	Low Definition
LWIR	Long-Wave Infrared
Mil.&Sur.	Military & Surveillance
MR	Magnetic Resonance
MWIR	Mid-Wave Infrared
NEP	Noise-Equivalent-Power
NIR	Near-Infrared
pri	Private Dataset
pub	Public Dataset
RGB	Red-Green-Blue
rr	Dataset that Requires Registration
SAR	Synthetic Aperture Radar
SD	Standard Definition
SNR	Signal-to-Noise Ratio
SWIR	Short-Wave Infrared
UHD	Ultra High Definition